Journal of the Geological Society

A detective duo of apatite and zircon geochronology for East Avalonia, Johnston Complex, Wales

Anthony J.I. Clarke, Christopher L. Kirkland & Stijn Glorie

Manuscript version: Accepted Manuscript

A detective duo of apatite and zircon geochronology for East Avalonia, Johnston Complex, Wales

Anthony J.I. Clarke [a], Christopher L. Kirkland [a], Stijn Glorie [b].

[a]Timescales of Mineral Systems Group, School of Earth and Planetary Sciences, Curtin University, GPO Box U1987, Perth, WA 6845, Australia.

[b]Department of Earth Sciences, University of Adelaide, Adelaide, South Australia, 5000, Australia.

Abstract

The Johnston Complex represents a rare inlier of the Neoproterozoic basement of southern Britain and offers a window into the tectonomagmatic regime of East Avalonia during the assembly of Gondwana. This work presents *in-situ* zircon (U-Pb, Lu-Hf), apatite (U-Pb), and trace element chemistry for both minerals from the Complex. Zircon and apatite yield a coeval crystallisation age of 570 ± 3 Ma, and a minor antecrystic zircon core component is identified at 615 ± 11 Ma. Zircon Lu-Hf data imply a broadly chondritic source, comparable to Nd data from East Avalonia, and T_{DM}^2 model ages of ca. 1.5 Ga indicate source extraction during the Mesoproterozoic. Zircon trace element chemistry is consistent with an ensialic calc-alkaline continental arc setting and demonstrates that magmatism was ongoing prior to terrane dispersal at 570 Ma. Apatite trace element chemistry implies a sedimentary component within the melt consistent with voluminous S-type granite production during the formation of Gondwana. The similarity of εHf and geochemistry between both zircon age populations suggest derivation from a uniform source that did not undergo significant modification between 615 – 570 Ma. Time-constrained apatite-zircon

chemistry addresses complexities in dating S-type granitoids (zircon inheritance) and permits inferences on post-magmatic thermal histories.

Highlights

- Coeval zircon-apatite demonstrates that calc-alkaline magmatism persisted in East Avalonia to ca. 570 Ma, prior to terrane dispersal.

- A uniform source melt from 615 to 570 Ma – a consistent position within the magmatic arc for the Cymru Terrane.

- A Mesoproterozoic T_{DM}^2 Lu-Hf model age of ca. 1.5 Ga for zircon, consistent with Sm-Nd data across East Avalonia.

- Coupled apatite–zircon geochronology can help address complexities within S-type granitoids (discerning primary vs inherited zircon) and clarify post-magmatic thermal histories.

Keywords: Neoproterozoic, U-Pb, Lu-Hf, geochemistry, Avalonia, Gondwana, southern Britain.

1.0. Introduction

The assembly of Gondwana over 800 – 550 Ma (Meert and Van Der Voo 1997) coincides with a crucial time in the evolution of Earth systems. Neoproterozoic lithologies provide evidence for the emergence of complex multicellular life (Shen *et al.* 2008), global glaciation (Shields-Zhou *et al.* 2016), and an important period of continental crust production in the Pan-African orogeny (Rino *et al.* 2008). Key to understanding these interrelated processes are paleotectonic reconstructions, which give constraints on the timing, duration, and style of magmatism. The construction of Gondwana was a protracted and complex process whereby microcontinents, such as Avalonia, were amalgamated onto and incorporated within the emerging landmass

(Cawood *et al.* 2021). The Neoproterozoic of southern Britain represents a prolonged (ca. 200 Ma) period of discontinuous magmatism, which necessitates accurate age-constrained isotopic and geochemical signatures to reconstruct the tectonic setting of Peri-Gondwanan terranes in this area (Pharaoh and Carney 2000; Compston *et al.* 2002; Schofield *et al.* 2016).

Drill-core and geophysical data indicate that England and Wales (south of the Iapetus suture) are underlain by a mosaic of Avalonian terranes, which from west to east include the Cymru, Wrekin, Charnwood and, Fenland terranes (Pharaoh and Carney 2000; McIlroy and Horak 2006; Schofield *et al.* 2016). However, complications arise from the sparsely-distributed, fault-uplifted tectonic inliers (Figure 1) and the varying degrees of deformation and metamorphism sustained by Precambrian basement lithologies during the Caledonian, Variscan, and Alpine orogenies (Pharaoh and Carney 2000). The Johnston Complex, the Arfon and Sarn Groups of North Wales, and the Pebidian Supergroup of North Pembrokeshire have been assigned to the Cymru Terrane (Pharaoh and Carney 2000; Schofield *et al.* 2016) (Figure 1). However, other workers have questioned the reliability of such broad terrane associations based on limited basement outcrops and the internal complexities of individual inliers (Compston *et al.* 2002; Schofield *et al.* 2016). The Johnston Complex typifies this issue; based on published zircon U-Pb ages and its calc-alkaline geochemistry, it has been alternatively classified into the Wrekin Terrane (McIlroy and Horak 2006) or Cymru Terrane (Figure 1) (Pharaoh and Carney 2000; Compston *et al.* 2002; Schofield *et al.* 2016). East Avalonian terranes are interpreted to represent remnants of a single late-Neoproterozoic subduction margin (Pharaoh *et al.* 1987). As such, constraining tectonomagmatic processes during this formative period in the evolution of Earth systems relies on accurate terrane designations, which in turn, underpin paleo-

continental reconstructions, essential to constraining the relationships between different planetary geochemical reservoirs during important intervals in Earth's history (Figure 1) (Nance et al., 2008; Strachan et al., 2007).

As there is a general paucity of recent isotopic studies, previous terrane classification work has relied on sparse isotopic and geochemical data (Figure 1) (Pharaoh and Carney 2000; Schofield *et al.* 2016). The Johnston Complex of southwest Wales is a case in point, with research into the Johnston Complex being limited to Cantrill *et al.* (1916), Thorpe (1972), and the isotopic analyses of Patchett and Jocelyn (1979) and Schofield *et al.* (2016). Despite representing some of the oldest rocks in southern Britain, with a reported zircon U-Pb age of 643 +5/-28 Ma (Patchett and Jocelyn 1979), little other isotopic data is available for the Complex, aside from a whole-rock Nd analysis undertaken by Schofield *et al.* (2016). Hence, the context of the Johnston Complex within the broader Peri-Gondwanan magmatic realm is yet to be fully determined. Several details remain unresolved, including the degree of heterogeneity within the Complex (single pluton vs composite magmatic body), the character of its source rocks, the relationship of the Complex to surrounding inliers, and its ultimate terrane classification.

This work presents *in-situ* zircon (U-Pb, Lu-Hf), apatite (U-Pb) and trace element data for both minerals from the Johnston Complex. Our results demonstrate that the Complex is a composite magmatic body composed of discrete quartz diorite plutons along its c. 20 km length. Our data show that calc-alkaline magmatism persisted in an ensialic setting in East Avalonia to ca. 570 Ma, prior to oblique convergence and terrane dispersal. We demonstrate that the source melt of the Johnston Complex was derived from a uniform and broadly chondritic source from 615 – 570 Ma, consistent with evolved εNd values from East Avalonia. The chemical data presented here

reinforce the classification of the Complex within the Cymru Terrane of East Avalonia and show an S-type component within the melt. We demonstrate that a combined apatite and zircon geochronology approach constrains inherited vs primary zircon within S-type granitoids and clarifies the post-magmatic history of an igneous body.

2.0. Geological Background

2.1. Regional Geology

The Menai Strait Fault separates the Precambrian geology of southern Britain into the Avalonian and Monian tectonic blocks (Figure 1) (Strachan *et al.* 2007; Woodcock *et al.* 2012; Schofield *et al.* 2016). Several terranes within these blocks (e.g., Cymru, Charnwood, Fenland and Wrekin) comprise the Avalon Composite Terrane, which is primarily concealed by Phanerozoic rocks (Pharaoh and Carney 2000; Schofield *et al.* 2016). Major fault zones, such as the Malvern Fault System and the Welsh Borderland Fault System, represent the broad structural controls on the distribution of Neoproterozoic inliers in southern Britain (Figure 1) (Pharaoh and Carney 2000; Woodcock *et al.* 2012). The ultimate relationship between the Avalonian and Monian terranes remains unresolved. However, both share a history of calc-alkaline magmatism, accretionary prism and basement gneiss amalgamation during the late Neoproterozoic (Woodcock *et al.* 2012; Schofield *et al.* 2016). Isotopic and structural data point towards a shared genesis for both units (Horak *et al.* 1996), and taken together, they are termed the Avalon Superterrrane.

2.2. Geology of the Johnston Complex

The Precambrian rocks of southwest Wales crop out in two areas north and south of St. Brides Bay (Figure 1). To the south is the Johnston Complex, an east-west trending intrusive suite of felsic plutons comprising diorites, tonalites, and granodiorites (Thorpe

1972). These rocks are cross-cut by metre-scale dolerite dykes emplaced during the Variscan orogeny (Thorpe 1972; Patchett and Jocelyn 1979; Thorpe 1979). The Johnston Complex is exposed in two outcrops: a coastal section on the southern end of St. Brides Bay and an inland area within the Bolton Hill Quarry near the eponymous town of Johnston (Figure 1). The Johnston Complex is thrust atop Palaeozoic sedimentary rocks and is entrained within the hanging wall of the Johnston-Benton thrust zone (Woodcock *et al.* 2012). The coastal outcrop of the Johnston Complex is comprised of quartz diorite, which is dominated by plagioclase (oligoclase to andesine), quartz, partially altered primary mafic minerals (hornblende and biotite) now occurring as chlorite, sericite and illite, and minor iron-titanium oxides (Figure 2).

There is some lithological variability between the inland portion and coastal outcrops. The inland lithologies have an increased abundance of hornblende and biotite, but alkali feldspar is mainly absent (Thorpe 1972; Thorpe 1979). In contrast, the coastal outcrops have a more homogenous quartz diorite composition and contain orthoclase at < 2% modal abundance (Thorpe 1972).

4.0. Methods

4.1. Mineral separation

A sample of quartz dolerite from the Johnston Complex was collected from south of St. Brides Bay (51°46'21.6"N 5°08'57.1"W). Zircon and apatite grains were separated following standard procedures at the John De Laeter Centre (JdLC), Curtin University. The sample was crushed using a ring mill and sieved to yield the ≤ 425 µm fraction. This fraction underwent heavy mineral separation via a Jasper Canyon Research water shaking table (Dumitru 2016). Lithium heteropolytungstate heavy liquid

separation at 2.85 g/cm^3 and Frantz isodynamic separation followed to produce a final fraction which was mounted in entirety onto a 25 mm epoxy resin round.

A polished 4 x 2 cm block was also prepared and analysed via a Tescan Integrated Mineral Analyser (TIMA) to provide insights into texture and mineralogy. Both the round mount and block were polished using a 1 μm diamond suspension fluid and imaged using reflected and transmitted light. TIMA analysis was used to identify mineral phases on the mount and block, and a Clara FE-SEM was then used to provide high-resolution images of internal grain morphology – aiding spot placement during LA-ICP-MS analysis.

4.2. Isotopic Analysis

4.2.1. Zircon U-Pb and Lu-Hf

A single session of split-stream zircon U-Pb and Lu-Hf analysis was undertaken at the GeoHistory Facility at the JdLC, Curtin University. A RESOlution LE193 nm ArF and a Lauren Technic S155 cell were used to ablate zircon with an Agilent 8900 ICPMS to collect U-Pb data, whilst Lu-Hf isotopes were collected simultaneously via a Nu Plasma II MC-ICPMS. The relatively small grain size of zircon (typically < 70 μm in length) and internal complexities necessitated a comparatively small spot size of ~38 μm diameter.

The matrix-matched primary reference material used for zircon U-Pb data reduction was GJ1 (Jackson *et al.* 2004). Plešovice, 337.13 ± 0.37 Ma; (Sláma *et al.* 2008) and 91500, 1063.78 ± 0.65 Ma; (Wiedenbeck *et al.* 1995) secondary reference materials were used to monitor the accuracy of the ^{238}U/^{206}Pb ratio measurement. To check the accuracy of ^{207}Pb/^{206}Pb ages, OG1, 3465.4 ± 0.6 Ma; (Stern *et al.* 2009) was reduced against Maniitsoq, 3008.70 ± 0.72 Ma; (Marsh et al., 2019). All weighted mean ages

for secondary reference materials were within 2σ uncertainty of accepted values (Appendix 1).

Mud Tank zircon (Woodhead *et al.* 2004) was the primary reference material for zircon Lu-Hf analyses. Several secondary reference zircon including GJ1, 0.282000 ± 0.000025; (Morel *et al.* 2008), 91500, 0.282306 ± 0.00004; (Woodhead *et al.* 2004; Woodhead and Hergt 2005) and R33, 0.282764 ± 0.000014; (Fisher *et al.* 2014a) were measured to confirm accuracy. All reference materials gave $^{176}Hf/^{177}Hf$ ratios within 2σ uncertainty of the accepted values, whilst the stable $^{178}Hf/^{177}Hf$ ratio was also within 2σ uncertainty of the expected ratio (Appendix 1) (Sláma *et al.* 2008; Fisher *et al.* 2014b).

4.2.2. Apatite U-Pb

Two sessions of apatite U-Pb isotopic analyses were completed at the GeoHistory Facility, JdLC, using a RESOlution 193 nm ArF with a Lauren Technic S155 cell and an Agilent 8900 ICPMS. Given the small-grain size (< 50 µm) of apatite from the Johnston Complex, a 38 µm spot size was ablated using a 5 Hz repetition rate and a fluence of ~ 2 J/cm^{-2}. Madagascar (MAD-2) (Thompson *et al.* 2016) and Mt. McClure (MMC) (Schoene and Bowring 2006) apatite were used as the primary reference material for sessions 1 and 2, respectively. Secondary reference material analysed included the MMC apatite (523.51 ± 1.47 Ma), Duluth Complex (FC) apatite (U-Pb zircon age of 1099.1 ± 0.2 Ma; (Schmitz et al., 2003) and the Durango apatite (31.44 ± 0.18 Ma) (McDowell *et al.* 2005). Ages obtained via unanchored regressions through the secondary reference apatite were within 2σ uncertainty of accepted ages (Appendix 2).

4.2.3. Apatite and Zircon Trace Elements

A single session of zircon and apatite trace elements was performed at the GeoHistory Facility at the JdLC. *In-situ* trace element measurements were made on some grains not previously analysed during earlier U-Pb sessions using an Agilent 8900 ICPMS. The size of zircon and apatite grains necessitated a 38 μm spot size at a fluence of 2.5 J/cm^{-2} and a 5 Hz laser pulse rate.

NIST 610 was used as the primary reference material for zircon analyses to calculate elemental abundance and correct for instrumental drift. The internal reference isotope used was ^{29}Si, assuming a stoichiometric zircon composition of 14.76 wt% silicon. Secondary reference materials included the 91500 zircon, using the reported values of Sano *et al.* (2002) and the NIST 612 (Jochum *et al.* 2005). For both reference materials, measured abundances were within 5 – 10% of reported values.

NIST 610 was the primary reference material for apatite trace element analyses. ^{29}Si was used as the internal reference isotope, assuming an apatite Si content of 0.41 wt% (Azadbakht *et al.* 2018). Secondary reference materials included the Durango apatite and NIST 621 glass; measured abundances were generally within 10% of reported values (Jochum *et al.* 2005; McDowell *et al.* 2005).

5.0. Results

5.1. Petrography

Automated mineralogy undertaken via TIMA is consistent with previous petrographic accounts of Cantrill *et al.* (1916) and Thorpe (1972). The Johnston Complex sample is a mesocratic medium-grained (1 – 5 mm) quartz diorite to tonalite principally composed of plagioclase feldspar (oligoclase to andesine) and quartz (Figure 2). Primary mafic minerals (hornblende and biotite) are variably altered to hydrous

secondary phases, including chlorite, sericite, and illite. Accessory minerals within this rock include apatite, zircon, muscovite, and iron-titanium oxides, including rutile and hematite (Figure 2). Orthoclase occurs at low modal abundances (<2%) within antiperthite textures. Veinlets of pumpellyite cross-cut the sample (Figure 2), consistent with the low-grade metamorphism experienced by the Complex and other Neoproterozoic inliers in southwest Wales (Thorpe 1972; Patchett and Jocelyn 1979). There is a general lack of significant metamorphic and deformational overprint on the sample, with only limited strained quartz, consistent with the rock fabric being dominantly magmatic.

5.2. Zircon

5.2.1. Zircon Morphology

Zircon grains from the Johnston Complex are colourless to light brown, tabular, euhedral to subhedral and are mainly intact crystals. Pristine grains have aspect ratios of ≥ 3:1. The grain size is variable but does not typically exceed 200 µm in length. Sharp, oscillatory zoning, with well-defined core-rim relationships (based on cathodoluminescence response), is apparent in the zircon population. Small anhedral ≤10 µm apatite inclusions are found within some zircon crystals.

Zircon grains are predominantly situated on the margins of quartz or are contained within plagioclase and quartz (Figure 3A-B). Zircon is also associated with altered hydrous phases such as chlorite (Figure 3A). A petrographic relationship between zircon and mafic minerals has been observed in many granitoids and attributed to enhanced local Zr saturation (Bacon 1989; Elburg 1996) or greater zircon growth potential in localised volatile-rich melt pockets (Miller *et al.* 2007; Erdmann *et al.* 2012). Zircon is absent in the late pumpellyite veinlets (Figure 3A).

5.2.2. Zircon U-Pb, Lu-Hf & Trace Elements

Over two analytical sessions, 124 U-Pb isotopic analyses were performed on zircon grains, from which 29 were less than 10% discordant. In Tera-Wasserburg plots, some zircon analyses scatter towards lower $^{238}U/^{206}Pb$ ratios at constant $^{207}Pb/^{206}Pb$, interpreted to reflect recent radiogenic-Pb loss (Figure 4).

The concordant analyses define two coherent groups of ages (Population 1 & 2). Group 1 yields a concordia age of 569 ± 2 Ma, n = 27, MSWD = 1.9, $p(x^2)$ = 0.079, which is interpreted as the magmatic crystallisation age for the quartz diorite, consistent with the oscillatory zoned zircon textures for this component (Figure 2).

Population 2 is defined by two zircon core analyses and is statistically distinct from Population 1, yielding an older concordia age of 615 ± 11 Ma, MSWD = 0.28, $p(x^2)$ = 0.89. Population 2 is interpreted to represent older cores and was exclusively collected from larger zircon grains, which permitted individual cores to be analysed (Figure 2). Given the low number of analyses, these grains could represent either rare inherited zircons assimilated from the wall rock or an antecrystic component from an earlier magmatic episode within the same longer-lived system igneous system. The similarity of zircon REE and Lu-Hf chemistry between Populations 1 and 2 supports the latter interpretation.

Zircon REE chondrite-normalised (Boynton 1984) plots show positively sloping gradients with cerium enrichment and europium depletion (Figure 5). The mean cerium anomaly (Ce/Ce*) for zircon from the Johnston Complex is +1.48, whilst the Eu anomaly $(Eu/Eu^*)_{CN}$ is strongly negative at 0.28. Some analyses show flattening of the light REE slope (LREE/MREE, $(La/Sm)_{CN}$), consistent with a gain of non-

stoichiometric elements into metamict zircon. These analyses typically yield discordant U-Pb isotopic results (Figure 4).

A total of 44 zircon Lu-Hf analyses were obtained (Figure 6). Analyses of concordant zircon yield εHf of -4.0 to 2.9 for Population 1 with a weighted mean of -0.41 ± 1.38 (MSWD = 0.68). Population 2 εHf values range from -4.0 to -1.2 (Figure 6). Both populations yield similar model ages with a mean Lu-Hf T_{DM}^2 of 1521 Ma.

5.3. Apatite

5.3.1 Apatite Morphology

Apatite from the Johnston Complex typically occurs as small (~ 50 μm) (Figure 3) subhedral, equant grains; however, the largest euhedral apatite is over 120 μm in length. Most grains are intact, with hexagonal basal sections. Apatite grains are largely colourless to light brown and internally homogenous without inclusions. Apatite is primarily associated with hydrous minerals (i.e., chlorite), and some grains occur within quartz, oligoclase and andesine (Figure 3).

5.3.2. Apatite U-Pb

A total of 94 apatite U-Pb analyses define a discordant array on the Tera Wasserburg concordia diagram spanning between a $^{207}Pb/^{206}Pb$ value of 0.85 ± 0.0086 at the upper intercept to an apparent age of 576 ± 11 Ma at the radiogenic lower intercept, MSWD = 1.2; $p(x^2)$ = 0.064. The F207% of apatite analyses range from 12 – 99%, with a mean value of 69% (Figure 4). F207% defines the distance along a mixing line between the non-radiogenic (common Pb) and radiogenic Pb component, where a higher % implies a greater common Pb component (Kirkland *et al.* 2017).

5.3.4. Apatite Trace Elements

The uranium concentration of the apatite ranges from 1.3 to 151.6 ppm, and the mean concentration is 9.2 ppm. Thorium concentrations range from 2.9 to 203.5 ppm, with a mean value of 25.8 ppm. REE chondrite-normalised plots (Boynton 1984) show a characteristic negative slope from light to heavy REE, with a median $(La/Sm)_{CN}$ value of 2.6. The europium anomaly (Eu/Eu^*) of the apatite is comparable to that in zircon at 0.35 (Figure 7).

6.0. Discussion

6.1. The Johnston Complex: A composite magmatic body

The ages yielded by population 1 zircon and apatite analyses are identical within uncertainty and yield a combined weighted mean age of 570 ± 3 Ma (MSWD = 1.5) (Figure 4), interpreted as the crystallisation age of the quartz diorite component of the Johnston Complex. This ca. 570 Ma age contrasts with the only previously reported U-Pb age for the Johnston Complex of 643 +5/-28 Ma (Patchett and Jocelyn 1979) (Figure 1). Previous workers, including Patchett and Jocelyn (1979) and Thorpe (1979), concluded that the entire Johnston Complex (aside from the dolerite dykes) was emplaced at ca. 643 Ma. Assuming that the multigrain zircon fractions reported by Patchett and Jocelyn (1979) reflect a magmatic event, the apparent ca. 643 Ma U-Pb age implies an earlier stage of magmatism for an inland component of the Johnson Complex. This interpretation is consistent with the observation that different multigrain size fractions of the Patchett and Jocelyn (1979) data set define a single lower intercept with no excess dispersion (Figure 4). Here, we also report an older ≥ 615 Ma antecrystic zircon core component (Population 2) within the coastal outcrop of the Complex (Figure 4).

In this work, we analysed a sample collected 9 km to the west of the study site of Patchett and Jocelyn (1979). Geophysical data and field observations show that both outcrops of the Complex are bound within the Johnston-Benton thrust zone and share a quartz diorite composition (Thorpe 1979; Woodcock *et al.* 2012). Therefore, our isotopic data indicate that the Complex represents discrete magmatic units with ages spanning over 40 Ma (Figure 4). Hence, previous accounts that the Complex represented a single magmatic episode at ca. 650 Ma (Pharaoh and Carney 2000; Woodcock *et al.* 2012; Valley *et al.* 2014) now appear inconsistent with the younger Cryogenian history of plutonism recorded within the apatite and zircon of the western Johnston Complex.

Neoproterozoic igneous activity in southern Britain has been summarised via a three-stage model (Pharaoh and Carney 2000; Woodcock *et al.* 2012). Based on the new geochronology reported herein, the Johnston Complex retains information from each stage (Figure 8). An early ca. 700 – 640 Ma period of magmatism is recorded throughout the basement of southern Britain and is characterised by pluton emplacement at mid-crustal depths within the Wrekin Terrane, e.g. Stanner-Hanter, Malverns (Figure 1) (Pharaoh and Carney 2000). The inland ca. 643 Ma pluton of the Johnston Complex (Patchett and Jocelyn 1979) thus brackets the end of this earliest stage of magmatism.

Calc–alkaline arc plutons (Sarn Complex, Arfon Group) and volcanic sequences (Pebidian Supergroup) dominated a later period of magmatism from ca. 620 – 585 Ma during the so-called Main Magmatic Event within the British Avalonian Terranes (Pharaoh and Carney 2000). The ca. 615 Ma zircon core age and ca. 570 Ma zircon and apatite U-Pb age (Figure 4) constrain the age of the western portion of the Johnston Complex to a hitherto unidentified younger expression of the Main Magmatic

Event. The ca. 615 Ma zircon core age is coeval with a 614 ± 2 Ma age reported for the Arfon Group (Figure 8) (Tucker and Pharaoh 1991), pointing towards an interval of calc-alkaline plutonism in the Cymru Terrane at this time (Schofield *et al.* 2016). Furthermore, zircon U-Pb data from the Fenland Terrane also record magmatism at 615 ± 6 Ma (Noble *et al.* 1993). Based on the shared ca. 615 Ma age and εNd signatures, Schofield *et al.* (2016) posited that the Fenland Terrane, Arfon and Sarn Complex were the disrupted remains of a single basement unit. The context of the Johnston Complex to this purported basement block remains enigmatic as we report only two ca. 615 Ma grain cores; nonetheless, it is noteworthy that magmatism of this age has not been documented from the Cymru, Wrekin, and Charnwood Terranes (Schofield *et al.* 2016).

Despite their close geographical proximity (Figure 1), the relationship between the Pebidian Group and Johnston Complex remains unresolved, and this has led to these two inliers having variable terrane classifications, see McIlroy and Horak (2006) cf. Pharaoh and Carney (2000). A minimum age of ca. 587 +25/-14 Ma is reported for the Pebidian Group from the cross-cutting St. David's granophyre (Patchett and Jocelyn 1979). The ca. 570 Ma age obtained from zircon and apatite in this study, combined with the strongly calc-alkaline affinities of both inliers, point towards a genetic relationship between the Pebidian Supergroup and Johnston Complex, thereby supporting the position of the Complex within the Cymru Terrane. If so, the coastal pluton of the Johnston Complex would be constrained to the final stage of magmatism, defined by the transition from a magmatic-dominated regime to one of sedimentation and oblique terrane dispersal (Pharaoh and Carney 2000; Woodcock *et al.* 2012).

McIlroy and Horak (2006) posited that the Welsh Borderland Fault System (WBFS, Figure 1) represented a terrane boundary between the Wrekin and Cymru Terrane.

The combined ca. 570 Ma apatite and zircon magmatic crystallisation age and their continental-arc geochemical signatures support the association of the Johnston Complex to the Cymru Terrane. Northern constituents of the Cymru Terrane (e.g., Arfon Group and Sarn Complex) share a geochemical affinity to the Pebidian Supergroup and Johnston Complex. To the east, the undated Coomb Volcanic Formation differs significantly, possessing intra-continental bimodal geochemical signatures (Figure 1) (Bevins *et al.* 1995). Other components of the Wrekin Terrane, such as the Longmyndian and Uriconian Groups, also share a pronounced intra-plate geochemistry, suggesting a decreasing influence of subduction-related magmatism towards the east (McIlroy and Horak 2006). We therefore suggest that the eastern margin of the Johnston Complex, the inferred extension of the Carreg Cennen Fault, is a terrane boundary separating the Cymru and Wrekin Terranes (Figure 1).

The relationship between the Benton Volcanic Group and the Johnston Complex is uncertain (Figure 1). Nonetheless, the entrainment of both inliers within the Johnston-Benton thrust zone and their shared calc-alkaline chemistry (Thorpe 1972; Bevins *et al.* 1995) implies a common magmatic source for both units. The rhyolitic lavas and tuffs of the Benton Group are posited to represent more evolved expressions of eruptives in the Pebidian Supergroup to the north (Baker 1982; Bevins *et al.* 1995). Given the potential linkage between the Pebidian and Johnston Complex, the Benton Group warrants further analysis to determine its broader terrane affinity and relationship to the Johnston Complex. The Johnston Complex now provides constraints on the evolution of the Cymru Terrane itself, representing some of the oldest ca. 640 Ma (Patchett and Jocelyn 1979) and youngest ca. 615 – 570 Ma magmatism in the area.

6.2. Geochemistry of the Johnston Complex

6.2.1. Zircon Geochemistry: Continental Magmatic Arc Affinities

Previous accounts of the geochemistry of the Cymru Terrane (Thorpe 1972; Pharaoh *et al.* 1987; Bevins *et al.* 1995) have reported calc-alkaline geochemical signatures consistent with subduction-related continental arc magmatism. New zircon and apatite data reinforce these earlier interpretations and provide insights into the geochemistry of late-Main Stage magmatism in the Cymru Terrane. The chondrite normalised (Boynton 1984) REE plots for zircon of the Johnston Complex show positively sloping trends with Ce and Sm enrichment and Pr and Eu depletion (Figure 5). Oxidised Ce^{4+} is more compatible with zircon than more reduced cations of Ce (Belousova *et al.* 2002a). Accordingly, the positive cerium anomaly (+1.48, Figure 5) is a broad reflection of the oxidised nature of the source magma for the Complex (Belousova *et al.* 2002a). Subduction-derived melts are typically oxidised, with the zircon Ce enrichment of the Johnston Complex analogous to the modern Indonesian subduction system (Woodcock *et al.* 2012; Bénard *et al.* 2018).

Zircon crystals derived from fractionated granitoid melts generally show a negative Eu anomaly, representing Eu^{2+} sequestration during oligoclase and andesine crystallisation. The zircon Eu anomaly reported here (0.28) is consistent with an evolved source melt and the high abundance of plagioclase within the quartz diorite of the Complex (Figure 2) (Appendix 1).

Geochemical data suggest that evolved calc-alkaline plutonism persisted in the Cymru Terrane to at least ca. 570 Ma, and the emplacement of the Johnston Complex was, therefore, contemporaneous with the terrane dispersal and oblique convergence associated with the final stage of Neoproterozoic magmatism in southern Britain

(Pharaoh and Carney 2000). The geochemical profiles of the Johnston Complex and the Pebidian Supergroup represent an archive of the evolving tectonic setting of the Cymru Terrane from a time of mid-crustal plutonism at ca. 640 – 615 Ma (Johnston Complex) to intercalated volcanism and sedimentation within the Welsh Basin during the Palaeozoic (Pebidian Supergroup). Late-Neoproterozoic < 580 Ma components of the Wrekin Terrane, such as the Uriconian and Warren House Groups, have geochemical affinities that shifted towards more intra-plate bi-modal components. Such geochemical trends point towards later arc-rifting, i.e. suggesting a more distal location from the subducting front for these units (Bevins *et al.* 1995; Pharaoh and Carney 2000). Our geochemical data (Figure 5) are consistent with the Johnston Complex retaining a uniform evolved calc-alkaline magmatic signature from ca. 640 to 570 Ma, suggesting a lack of source magma modification prior to terrane dispersal after ca. 570 Ma.

6.2.2. Apatite Geochemistry: Gondwanan S-type Granite Production

Unlike zircon from the Johnston Complex, apatites do not show a pronounced Ce anomaly (Ce/Ce* = 0.02) (Figure 7). Such a trend is typical in evolved felsic melts, where Ce is sequestered into fractionating plagioclase (London 1992). Although Ce sequestration can occur into epidote-group minerals (Glorie *et al.* 2019), this process appears minimal in the Johnston Complex, given the absence of primary epidote-group minerals or allanite (Figure 2).

Sha and Chappell (1999) demonstrated that apatites in S-type and I-type granites show a chondrite-normalised depletion in Th and LREEs and, thus, a shallower slope, which flattens with increasing atomic mass in REE plots (Figure 7). Conversely, I-type granites can typically show a distinct enrichment in LREE and HREEs, compared to U and MREEs – a trend not evident in apatite from the Johnston Complex. Instead, the

apatite has a negatively sloping REE trend, with a moderate negative Eu anomaly of 0.35 and a mean $(Ce/Yb)_{cn}$ of 7.3, typical of apatite grains derived from evolved granitoids (Figure 7) (Sha and Chappell 1999; Belousova *et al.* 2002b; Chu *et al.* 2009). Accordingly, the Johnston Complex apatite falls within the range of S-type granites compiled by O'Sullivan *et al.* (2020) (Figure 7). The mineralogy of the Johnston Complex is also consistent with an S-type source, including apatite being relatively abundant (~0.20% modal abundance) and an absence of diagnostic minerals for I-type granites such as allanite and magnetite (Chappell and White 2001). The predominant association of zircon within altered mafic minerals (chlorite and hornblende) in the Complex (Figure 3) is also consistent with an S-type classification (Clemens *et al.* 2016).

Continental arc granitoids, such as the Johnston Complex, typically form by melting pre-existing crust, with potential input from juvenile material (Hawkesworth *et al.* 2010). I-type felsic melts can transition to a more peraluminous composition following assimilation with material derived from subduction, such as greywackes and shales (Chappell and White 2001). Extensive continental collision and orogenesis, associated with the assembly of Gondwana, were posited to have led to the uplift and production of giant turbidite fans (Zhu *et al.* 2020). Erosion of the uplifted hinterland supported prolonged delivery of supracrustal detritus via subduction-related erosion followed by transfer to the upper plate. Our data suggest the Johnston Complex, an S-type granite from a peri-Gondwanan terrane, is a consequence of this process.

6.2.3. Coupled Apatite-Zircon Analyses in S-type Granitoids

Obtaining primary magmatic crystallisation ages can be challenging for S-type granites due to the common presence of inherited zircons, with difficulties in definitively identifying neoblastic growth in such rocks (Collins *et al.* 2021; Kelsey *et al.* 2022).

Differentiating primary vs inherited zircon has important implications for accurate terrane classification, where zircon U-Pb crystallisation ages are often the key discrimination or association parameter between disparate inliers (Pharaoh and Carney 2000; Schofield *et al.* 2016).

Given solubility considerations, apatite is much less likely to be an inherited phase in felsic melts than zircon (Wolf and London 1994). Where both zircon and apatite yield similar crystallisation ages, and the host rock shows little evidence of recrystallisation, this provides a compelling case for coeval magmatic growth. Coeval ages for both minerals also imply rapid cooling (i.e. shallow, epizonal emplacement) through the radiogenic Pb closure temperature of both minerals (zircon ≥ 900°C and apatite ≥ 350°C) (Figure 4) (Chew and Spikings 2021).

Apatite and zircon ages at ca. 570 Ma for the Johnston Complex imply that calc-alkaline magmatism was ongoing during the final stages of Eastern Avalonian arc magmatism in the Cymru Terrane (Woodcock *et al.* 2012). Across the inliers of southern Britain, an absence of calc-alkaline magmatism post ca. 570 Ma has been attributed to the increasingly oblique convergence of East Avalonia with Laurentia and the detachment of coherent geology into tectonic slivers and subsequent terrane dispersal (Figure 9) (Horak *et al.* 1996; Woodcock *et al.* 2012). The rapid cooling of the Johnston Complex at ca. 570 Ma and its low metamorphic grade is consistent with structurally controlled emplacement into the shallow crust. Increasing rates of oblique convergence and transpression along strike-slip faults have been proposed to reduce the geothermal gradient of mid to upper-crustal sections (Alvarado *et al.* 2016; Collett *et al.* 2019). Hence, the 570 Ma age of the Johnston Complex is consistent with Eastern Avalonian terrane dispersal along the subduction front (Woodcock *et al.* 2012). During this process, strike-slip faults would have provided conduits for melt

emplacement and crystallization of the Johnston Complex at shallow, epizonal, depths (Murphy *et al.* 2022).

In addition, these new data imply that the Johnston Complex has undergone minimal thermal disturbance following magmatic crystallisation at ca. 570 Ma. The U-Pb closure temperature of apatite is highly dependent on microstructures, grain size and cooling rates. Consequently, reported closure temperatures range between 350 – 600°C (Chew and Spikings 2015; Kirkland *et al.* 2018). Nonetheless, apatite U-Pb ages typically represent metamorphic perturbances at mid to upper-crust conditions or protracted cooling through the closure temperature range (Chew and Spikings 2015; Kirkland *et al.* 2018; Gillespie *et al.* 2022). The similarity between apatite and zircon U-Pb ages implies that the Johnston Complex cannot have resided at temperatures ≥ 350°C for a protracted period. Rather, the isotopic data imply rapid cooling through both minerals' U-Pb closure temperatures. Rapid cooling at a relatively shallow depth of emplacement is consistent with the coeval crystallisation of apatite and zircon within this constituent body of the Johnston Complex (Figure 1).

K-Ar hornblende data from another coastal outcrop of the Complex has yielded ca. 612 – 624 Ma ages, and biotite from the Dutch Gin series, a so-called metre-scale band of localised deformation at the western margin of the Complex, yields a K-Ar date of ca. 612 Ma (Thorpe 1979). The relatively lower closure temperature of the K-Ar system in both minerals (300 – 600°C) (Harrison 1982) further suggests that the Complex experienced minimal post-magmatic thermal perturbations. The Johnston Complex is now bound within a Variscan thrust zone and was also emplaced prior to the Caledonian orogeny, yet neither tectonic event caused extensive metamorphism of the Complex (Thorpe 1972; Patchett and Jocelyn 1979). Indeed, across the

Neoproterozoic rocks of southwest Wales metamorphism is limited to prehnite-pumpellyite facies (Figure 1) (Thorpe 1972).

6.3. Zircon Lu-Hf: A Mesoproterozoic source melt?

Zircon εHf data for ca. 570 Ma crystals (Population 1) forms a broadly sub-chondritic cluster, with a mean εHf of -0.41 ± 1.38. The older ca. 615 Ma (Population 2) cores have εHf values that are not significantly different (Figure. 5), suggesting that both magmatic episodes were derived from compositionally similar sources (at least in terms of Lu/Hf ratio) that did not undergo significant evolution or modification during the ca. 615 – 570 Ma interval.

A Lu/Hf ratio of 0.05 was chosen to reflect a felsic source for the parental melt of the Johnston Complex, consistent with other S-type Proterozoic granitoids from the database compiled by Bea *et al.* (2018). Two-stage depleted mantle Lu-Hf model ages (T_{DM}^2) imply late Mesoproterozoic 1011 – 1892 Ma crust-extraction dates, with a mean T_{DM}^2 of 1521 Ma. Model ages, especially in the case of S-type granitoids, may only provide a minimum age for the oldest component within a mixed magma. Nonetheless, the zircon Hf isotopic signature, with a source crustal residence time of at least 800 – 500 Ma, is similar to other Avalonian granitoids (Figure 6) (Pollock *et al.* 2015; Henderson *et al.* 2016; Schofield *et al.* 2016).

A whole-rock εNd value of -1.8 with a T_{DM}^2 of 1437 Ma was reported for the Johnston Complex from the inland outcrop (Schofield *et al.* 2016). Along with the Lu-Hf T_{DM}^2 for zircon reported here, these data imply variable degrees of crustal contamination. Complementary εHf data from Western Avalonia granitoids yield analogous late Mesoproterozoic T_{DM}^2 ages implying a similar source for most Avalonian micro-

continental blocks during the late Neoproterozoic (Figure 6) (Willner *et al.* 2013; Pollock *et al.* 2015; Henderson *et al.* 2016).

Although localised areas of considerably older Proterozoic ≥ 1.6 Ga crust in West Avalonia have been inferred by εHf data (Willner *et al.* 2013; Pollock *et al.* 2015; Henderson *et al.* 2016), there is no evidence of similarly ancient crust based on the sparse Lu-Hf dataset for the Cymru Terrane. Nonetheless, the presence of older, mid-Proterozoic crustal components within the Cymru Terrane is implied by Sm-Nd model ages of ca. >1.35 Ga for the Parwyd Gneisses and Sarn Granites (Figure 1) (McIlroy and Horak 2006). Other areas show more definitive evidence of older underlying crust. For example, the Malverns Complex (Figure 1) has yielded inherited zircon age maxima of ca. 1.6 Ga and whole-rock Sm-Nd model ages of ca. 1.4 – 1.6 Ga (Murphy *et al.* 2000; McIlroy and Horak 2006). Such older crustal components provide an important distinction between the Cymru and Wrekin Terranes, in which the latter appears to incorporate an older crustal component.

Zircon data from other East Avalonian lithologies also show similar εHf patterns to the Johnston Complex. For example, zircon grains from the Stavelot-Venn Massif of East Avalonia imply felsic melt generation from a chondritic source of similar age and composition to the Johnston Complex (Figure 6) (Willner *et al.* 2013). Hence, εHf data from the Johnston Complex, when considered with data from other terranes, support the interpretation that Avalonian terranes formed from a relatively uniform Neoproterozoic continental arc system with a broadly chondritic melt source (Figure 6) (Pollock *et al.* (2015) variably contaminated with older Meso to Paleoproterozoic crust (e.g. Wrekin Terrane) (Thorpe *et al.* 1984). This contamination could represent localised input into the subduction system of allochthonous structurally emplaced older crust during the Proterozoic (Pollock *et al.* 2015).

7.0. Conclusion

New time-constrained (U-Pb) isotopic (Lu-Hf) and trace element data from the Johnston Complex, Wales, help constrain magmatism in East Avalonia during the late Neoproterozoic. We report ages for a coastal pluton of the Complex from coeval apatite and zircon at 570 ± 3 Ma. Combined with a previously reported age of ca. 643 Ma for an inland component, we demonstrate that the Complex is a composite suite of quartz diorite plutons along its ca. 20 km length. Our data necessitate that calc-alkaline igneous activity was ongoing to ca. 570 Ma in East Avalonia.

Apatite and zircon geochemistry provide complementary insights into late Neoproterozoic magmatism in southern Britain. Zircon trace elements demonstrate an oxidised calc-alkaline source magma typical of an ensialic subduction belt setting for the Complex. A sedimentary component within the melt is revealed through apatite trace element profiles – consistent with voluminous S-type granitoid production during the assembly of Gondwana. εHf values imply a broadly chondritic source melt for both zircon populations with a mean $T_{DM}{}^2$ of 1.5 Ga.

Classification of the Precambrian terranes of southern Britain has primarily been facilitated through correlating geochemical signatures, structural relationships, and Nd (model) ages. Generally, sparse U-Pb magmatic crystallisation dates have underpinned associations of otherwise disparate lithologies into unified terranes. Given this approach, the presented work offers a cautionary note. On the km scale, the Johnston Complex varies in age by over ca. 40 Ma (Figure. 3). Although individual zircon grains trace a multi-stage history with components at ca. 615 and 570 Ma, the combined zircon-apatite approach gives confidence in magmatic age assignment and facilitates terrane association in partially obscured basement areas.

Thus, in situations when the closure temperature of Pb in apatite has not been exceeded, the application of combined zircon and apatite geochronology may remove some ambiguity related to zircon inheritance when dating rocks.

Acknowledgments

Figure Captions

Figure 1. The distribution of Precambrian outcrops in southern Britain. Previous ages obtained include (a) Patchett and Jocelyn (1979) and (b) Unpublished K-Ar ages for muscovite and hornblende discussed by Patchett and Jocelyn (1979). The schematic tectonic map of southern Britain is adapted after Pharaoh and Carney (2000). The inset map of Precambrian geology in Pembrokeshire is modified after Bloxam and Dirk (1988). The coordinate system used is British National Grid. Abbreviations include WBFS = Welsh Borderland Fault System and MSFS = Menai Strait Fault System. Data sources are listed in superscript letters and include: a) Patchett and Jocelyn (1979), b) Tucker and Pharaoh (1991), c) Horak *et al.* (1996), d) Thorpe *et al.* (1984), e) Schofield *et al.* (2010), f) Noble *et al.* (1993), g) Beckinsale *et al.* (1984), h) Strachan *et al.* (1996), i) (Compston *et al.* 2002).

Figure 2. **Top Row:** Backscatter electron images of representative apatite, with a 38 µm spot and F207 corrected age shown. **Bottom Row:** Cathodoluminescence Images of zircon, with concordia ages and the 38 µm spot obtained from separate sessions shown. **Bottom Figure:** A TIMA phase map of minerals with a mass % above 0.10 for the quartz diorite of the Johnston Complex.

Figure 3. Compilation of representative backscatter electron images showing zircon and apatite mineral associations. Abbreviations: Andes = Andesine, Ap = Apatite, Chl = Chlorite, Ilm = Ilmenite, Olg = Oligoclase, Pmp = Pumpellytite, Qtz = Quartz, Rt = Rutile and Zr = Zircon.

Figure 3. Tera-Wasserburg plot for zircon and apatite of the Johnston Complex. Note the different precisions of U-Pb analyses across each session, a function of LA-ICP-MS counting time during U-Pb, and trace elements compared to split-stream U-Pb and Lu-Hf. The inset shows the lower intercept of the apatite U-Pb regression, a magnified view of zircon U-Pb analyses, and the earlier TIMS results of Patchett and Jocelyn (1979).

Figure 4. Zircon geochemistry discrimination diagrams. **A)** REE Chondrite normalised zircon multi-element plot (Boynton 1984). **B-D)** Bivariate plots of zircon geochemistry with compositional reference fields after Grimes *et al.* (2015). **E)** Eu/Eu* vs Ce/Ce* anomalies. Compositional reference fields adapted from Belousova *et al.* (2002a).

Figure 5. εHf plot for zircon of the Johnston Complex and other Avalonian Terranes. Data contoured using a kernel bandwidth of 10 for the X-axis and 1.25 intervals for the Y-axis. εHf data compiled from Pollock *et al.* (2015) and Willner *et al.* (2013).

Figure 6. Apatite geochemistry discrimination diagrams. **A)** REE chondrite normalised apatite multi-element plot (Boynton 1984). Compositional data for granitoids from

O'Sullivan *et al.* (2020). **B)** Bivariate plot of the mean europium anomaly $(Eu/Eu^*)_c$ vs chondrite normalised Sm/Nd_c. Contoured compositional fields after Sha and Chappell (1999). **C)** Bivariate plot of apatite Th vs Ce abundance. Compositional reference fields adapted after Belousova *et al.* (2002b).

Figure 7. A stratigraphic terrane correlation chart of select areas adapted after Pharaoh and Carney (2000). Abbreviations include WBFS = Welsh Borderland Fault System, SHC = Stanner-Hanter Complex, THG = Twt Hill Group, SDG = St. David's Granophyre, BH = Bore-hole data, EG = Ercall Granophyre, JBTZ = Johnston Benton Thrust Zone. Data sources are listed in superscript letters and include: a) Patchett and Jocelyn (1979), b) Tucker and Pharaoh (1991), c) Horak *et al.* (1996), d) Thorpe *et al.* (1984), e) Schofield *et al.* (2010), f) Noble *et al.* (1993), g) Beckinsale *et al.* (1984), h) Strachan *et al.* (1996), i) Compston *et al.* (2002).

Figure 8. Schematic model showing the late-Neoproterozoic evolution of the Johnston Complex within the East Avalonian tectonic regime. Model adapted after Horak *et al.* (1996) and Pharaoh and Carney (2000). Abbreviations include: WBFS = Welsh Borderland Fault System, MSFS = Menai Strait Fault System, ML = Malverns Lineament, A= Arfon Group, B= Anglesey Blueschists, BG = Bwlch Gwyn Tuff, BV = Benton Volcanic Group, C = Coedana Complex, Ch = Charnian Supergroup, J = Johnston Complex, P = Pebidian Supergroup, O-G = Orton and Glinton Bore holes, R = Rosslare Complex, S = Sarn Complex, S-H = Stanner-Hanter Complex, U-E-L = Uriconian Volcanics, Ercall Granophyre, Longmyndian Supergroup, WH = Warren House Volcanics.

References

Alvarado, A., Audin, L. *et al.* 2016. Partitioning of oblique convergence in the Northern Andes subduction zone: Migration history and the present-day boundary of the North Andean Sliver in Ecuador. *Tectonics*, **35**, 1048-1065, https://doi.org/https://doi.org/10.1002/2016TC004117.

Azadbakht, Z., Lentz, D. and McFarlane, C. 2018. Apatite Chemical Compositions from Acadian-Related Granitoids of New Brunswick, Canada: Implications for Petrogenesis and Metallogenesis. *Minerals*, **8**, https://doi.org/10.3390/min8120598.

Bacon, C.R. 1989. Crystallization of accessory phases in magmas by local saturation adjacent to phenocrysts. *Geochimica et Cosmochimica Acta*, **53**, 1055-1066, https://doi.org/https://doi.org/10.1016/0016-7037(89)90210-X.

Baker, J.W. 1982. The Precambrian of south-west Dyfed, south-west Wales. *In*: Bassett, M.G. (ed.) *Geological excursions in Dyfed, south-west Wales*. National Museum of Wales, Cardiff, 15-25.

Bea, F., Montero, P., Molina, J.F., Scarrow, J.H., Cambeses, A. and Moreno, J.A. 2018. Lu-Hf ratios of crustal rocks and their bearing on zircon Hf isotope model ages: The effects of accessories. *Chemical Geology*, **484**, 179-190, https://doi.org/https://doi.org/10.1016/j.chemgeo.2017.11.034.

Beckinsale, R.D., Evans, J.A., Thorpe, R.S., Gibbons, W. and Harmon, R.S. 1984. Rb-Sr whole-rock isochron ages, $\delta^{18}O$ values and geochemical data for the Sarn Igneous Complex and the Parwyd gneisses of the Mona Complex of Llŷn, N Wales. *Journal of the Geological Society*, **141**, 701-709, https://doi.org/10.1144/gsjgs.141.4.0701.

Belousova, E., Griffin, W., O'Reilly, S.Y. and Fisher, N. 2002a. Igneous zircon: trace element composition as an indicator of source rock type. *Contributions to Mineralogy and Petrology*, **143**, 602-622, https://doi.org/10.1007/s00410-002-0364-7.

Belousova, E., Griffin, W., O'Reilly, S.Y. and Fisher, N. 2002b. Apatite as an indicator mineral for mineral exploration: Trace-element compositions and their relationship to host rock type. *Journal of Geochemical Exploration*, **76**, 45-69, https://doi.org/10.1016/S0375-6742(02)00204-2.

Bénard, A., Klimm, K. *et al.* 2018. Oxidising agents in sub-arc mantle melts link slab devolatilisation and arc magmas. *Nature Communications*, **9**, 3500, https://doi.org/10.1038/s41467-018-05804-2.

Bevins, R., Pharaoh, T., Cope, J. and Brewer, T. 1995. Geochemical character of Neoproterozoic volcanic rocks in southwest Wales. *Geological Magazine*, **132**, 339-349, https://doi.org/10.1017/S0016756800013649.

Bloxam, T.W. and Dirk, M.H.J. 1988. The petrology and geochemistry of the St. David's Granophyre and the Cwm Bach Rhyolite, Pembrokeshire, Dyfed. *Mineralogical Magazine*, **52**, 563-575, https://doi.org/doi:10.1180/minmag.1988.052.368.02.

Boynton, W.V. 1984. Chapter 3 - Cosmochemistry of the Rare Earth Elements: Meteorite Studies. *In*: Henderson, P. (ed.) *Developments in Geochemistry*. Elsevier, 63-114, https://doi.org/https://doi.org/10.1016/B978-0-444-42148-7.50008-3.

Cantrill, T.C., Dixon, E.E.L., Thomas, H.W. and Jones, O.T. 1916. *The geology of the south Wales Coalfield, Part XII, The country around Milford.* His Majesty's Stationery Office.

Cawood, P.A., Martin, E.L., Murphy, J.B. and Pisarevsky, S.A. 2021. Gondwana's interlinked peripheral orogens. *Earth and Planetary Science Letters*, **568**, https://doi.org/https://doi.org/10.1016/j.epsl.2021.117057.

Chappell, B.W. and White, A.J.R. 2001. Two contrasting granite types: 25 years later. *Australian Journal of Earth Sciences*, **48**, 489-499, https://doi.org/10.1046/j.1440-0952.2001.00882.x.

Chew, D.M. and Spikings, R.A. 2015. Geochronology and Thermochronology Using Apatite: Time and Temperature, Lower Crust to Surface. *Elements*, **11**, 189-194, https://doi.org/10.2113/gselements.11.3.189.

Chew, D.M. and Spikings, R.A. 2021. Apatite U-Pb Thermochronology: A Review. *Minerals*, **11**, https://doi.org/10.3390/min11101095.

Chu, M.F., Wang, K.L., Griffin, W., Chung, S.L., O'Reilly, S.Y., Pearson, D.G. and Iizuka, Y. 2009. Apatite Composition: Tracing Petrogenetic Processes in Transhimalayan Granitoids. *Journal of Petrology*, **50**, 1829-1855, https://doi.org/10.1093/petrology/egp054.

Clemens, J.D., Buick, I.S. and Kisters, A.F.M. 2016. The Donkerhuk batholith, Namibia: A giant S-type granite emplaced in the mid crust, in a fore-arc setting. *Journal of the Geological Society*, **174**, 157-169, https://doi.org/10.1144/jgs2016-028.

Collett, C.M., Duvall, A.R., Flowers, R.M., Tucker, G.E. and Upton, P. 2019. The Timing and Style of Oblique Deformation Within New Zealand's Kaikōura Ranges

and Marlborough Fault System Based on Low-Temperature Thermochronology. *Tectonics*, **38**, 1250-1272, https://doi.org/https://doi.org/10.1029/2018TC005268.

Collins, W.J., Murphy, J.B., Blereau, E. and Huang, H.Q. 2021. Water availability controls crustal melting temperatures. *Lithos*, **402-403**, 106351, https://doi.org/https://doi.org/10.1016/j.lithos.2021.106351.

Compston, W., Wright, A.E. and Toghill, P. 2002. Dating the Late Precambrian volcanicity of England and Wales. *Journal of the Geological Society*, **159**, 323-339, https://doi.org/10.1144/0016-764901-010.

Dumitru, T.A. 2016. A New Zircon Concentrating Table Designed for Geochronologists. presented at the American Geophysical Union, December 01, 2016, San Francisco.

Elburg, M.A. 1996. U-Pb ages and morphologies of zircon in microgranitoid enclaves and peraluminous host granite: evidence for magma mingling. *Contributions to Mineralogy and Petrology*, **123**, 177-189, https://doi.org/10.1007/s004100050149.

Erdmann, S., Wodicka, N., Jackson, S. and Corrigan, D. 2012. Zircon textures and composition: Refractory recorders of magmatic volatile evolution? *Contributions to Mineralogy and Petrology*, **165**, https://doi.org/10.1007/s00410-012-0791-z.

Fisher, C.M., Vervoort, J.D. and DuFrane, S.A. 2014a. Accurate Hf isotope determinations of complex zircons using the "laser ablation split stream" method. *Geochemistry, Geophysics, Geosystems*, **15**, 121-139, https://doi.org/https://doi.org/10.1002/2013GC004962.

Fisher, C.M., Vervoort, J.D. and Hanchar, J.M. 2014b. Guidelines for reporting zircon Hf isotopic data by LA-MC-ICPMS and potential pitfalls in the interpretation of these data. *Chemical Geology*, **363**, 125-133, https://doi.org/https://doi.org/10.1016/j.chemgeo.2013.10.019.

Gillespie, J., Kirkland, C.L., Kinny, P.D., Simpson, A., Glorie, S. and Rankenburg, K. 2022. Lu–Hf, Sm–Nd, and U–Pb isotopic coupling and decoupling in apatite. *Geochimica et Cosmochimica Acta*, **338**, 121-135, https://doi.org/https://doi.org/10.1016/j.gca.2022.09.038.

Glorie, S., Jepson, G. *et al.* 2019. Thermochronological and geochemical footprints of post-orogenic fluid alteration recorded in apatite: Implications for mineralisation in the Uzbek Tian Shan. *Gondwana Research*, **71**, 1-15, https://doi.org/10.1016/j.gr.2019.01.011.

Grimes, C.B., Wooden, J.L., Cheadle, M.J. and John, B.E. 2015. "Fingerprinting" tectono-magmatic provenance using trace elements in igneous zircon. *Contributions to Mineralogy and Petrology*, **170**, 46, https://doi.org/10.1007/s00410-015-1199-3.

Harrison, T.M. 1982. Diffusion of ^{40}Ar in hornblende. *Contributions to Mineralogy and Petrology*, **78**, 324-331, https://doi.org/10.1007/BF00398927.

Hawkesworth, C.J., Dhuime, B., Pietranik, A.B., Cawood, P.A., Kemp, A.I.S. and Storey, C.D. 2010. The generation and evolution of the continental crust. *Journal of the Geological Society*, **167**, 229-248, https://doi.org/10.1144/0016-76492009-072.

Henderson, B.J., Collins, W.J., Murphy, J.B., Gutierrez-Alonso, G. and Hand, M. 2016. Gondwanan basement terranes of the Variscan–Appalachian orogen: Baltican, Saharan and West African hafnium isotopic fingerprints in Avalonia, Iberia and the Armorican Terranes. *Tectonophysics*, **681**, 278-304, https://doi.org/https://doi.org/10.1016/j.tecto.2015.11.020.

Horak, J., Doig, R., Evans, J. and Gibbons, W.D. 1996. Avalonian magmatism and terrane linkage: New isotopic data from the Precambrian of North Wales. *Journal of the Geological Society*, **153**, 91-99, https://doi.org/10.1144/gsjgs.153.1.0091.

Jackson, S.E., Pearson, N.J., Griffin, W.L. and Belousova, E.A. 2004. The application of laser ablation-inductively coupled plasma-mass spectrometry to in situ U–Pb zircon geochronology. *Chemical Geology*, **211**, 47-69, https://doi.org/https://doi.org/10.1016/j.chemgeo.2004.06.017.

Jochum, K.P., Nohl, U., Herwig, K., Lammel, E., Stoll, B. and Hofmann, A.W. 2005. GeoReM: A New Geochemical Database for Reference Materials and Isotopic Standards. *Geostandards and Geoanalytical Research*, **29**, 333-338, https://doi.org/https://doi.org/10.1111/j.1751-908X.2005.tb00904.x.

Kelsey, D.E., Wingate, M. *et al.* 2022. *Crystalline basement beneath the eastern Canning Basin at the Top Up Rise prospect*. Geological Survey of Western Australia, Perth.

Kirkland, C.L., Hollis, J., Danišík, M., Petersen, J., Evans, N.J. and McDonald, B.J. 2017. Apatite and titanite from the Karrat Group, Greenland; implications for charting the thermal evolution of crust from the U-Pb geochronology of common Pb-bearing phases. *Precambrian Research*, **300**, 107-120, https://doi.org/10.1016/j.precamres.2017.07.033.

Kirkland, C.L., Yakymchuk, C., Szilas, K., Evans, N., Hollis, J., McDonald, B. and Gardiner, N.J. 2018. Apatite: a U-Pb thermochronometer or geochronometer? *Lithos*, **318-319**, 143-157, https://doi.org/10.1016/j.lithos.2018.08.007.

London, D. 1992. Phosphorus in S-type magmas: The P_2O_5 content of feldspars from peraluminous granites, pegmatites, and rhyolites. *American Mineralogist*, **77**, 126-145.

McDowell, F., McIntosh, W. and Farley, K. 2005. A precise $^{40}Ar–^{39}Ar$ reference age for the Durango apatite (U–Th)/He and fission-track dating standard. *Chemical Geology*, **214**, 249-263, https://doi.org/10.1016/j.chemgeo.2004.10.002.

McIlroy, D. and Horak, J. 2006. The Neoproterozoic of England and Wales. *In*: Brenchly, P.J. and Rawson, P.F. (eds) *The Geology of England and Wales*. Geological Society of London, London, 9-24.

Meert, G.J. and Van Der Voo, R. 1997. The assembly of Gondwana 800-550 Ma. *Journal of Geodynamics*, **23**, 223-235, https://doi.org/https://doi.org/10.1016/S0264-3707(96)00046-4.

Miller, J.S., Matzel, J.E.P., Miller, C.F., Burgess, S.D. and Miller, R.B. 2007. Zircon growth and recycling during the assembly of large, composite arc plutons. *Journal of Volcanology and Geothermal Research*, **167**, 282-299, https://doi.org/https://doi.org/10.1016/j.jvolgeores.2007.04.019.

Morel, M.L.A., Nebel, O., Nebel-Jacobsen, Y., Miller, J. and Vroon, P.Z. 2008. Hafnium isotope characterization of the GJ-1 zircon reference material by solution and laser-ablation MC-ICPMS. *Chemical Geology*, **255**, 231-235, https://doi.org/10.1016/j.chemgeo.2008.06.040.

Murphy, J.B., Collins, W.J. and Archibald, D.B. 2022. Logan Medallist 7. Appinite Complexes, Granitoid Batholiths and Crustal Growth: A Conceptual Model. *Geoscience Canada*, **49**, 237-249, https://doi.org/10.12789/geocanj.2022.49.191.

Murphy, J.B., Strachan, R.A., Nance, R.D., Parker, K.D. and Fowler, M.B. 2000. Proto-Avalonia: A 1.2–1.0 Ga tectonothermal event and constraints for the evolution of Rodinia. *Geology*, **28**, 1071-1074.

Noble, S.R., Tucker, R.D. and Pharaoh, T.C. 1993. Lower Palaeozoic and Precambrian igneous rocks from eastern England, and their bearing on late Ordovician closure of the Tornquist Sea: constraints from U-Pb and Nd isotopes. *Geological Magazine*, **130**, 835-846, https://doi.org/10.1017/S0016756800023190.

O'Sullivan, G., Chew, D.M., Kenny, G., Henrichs, I. and Mulligan, D. 2020. The trace element composition of apatite and its application to detrital provenance studies. *Earth-Science Reviews*, **201**, https://doi.org/10.1016/j.earscirev.2019.103044.

Patchett, P.J. and Jocelyn, J. 1979. U–Pb zircon ages for late Precambrian igneous rocks in South Wales. *Journal of the Geological Society*, **136**, 13-19, https://doi.org/10.1144/gsjgs.136.1.0013.

Pharaoh, T.C. and Carney, J.N. 2000. Introduction to the Precambrian Rocks of England and Wales. *In*: Carney, J.N. (ed.) *Geological Conservation Review Series.* Joint Nature Conservation Committee, Peterborough, 252.

Pharaoh, T.C., Webb, P.C., Thorpe, R.S. and Beckinsale, R.D. 1987. Geochemical Evidence for the Tectonic Setting of Late Proterozoic Volcanic Suites in Central England. *Geological Society, London, Special Publications*, **33**, 541-552, https://doi.org/10.1144/GSL.SP.1987.033.01.36.

Pollock, J., Sylvester, P. and Barr, S.M. 2015. Lu–Hf zircon and Sm–Nd whole-rock isotope constraints on the extent of juvenile arc crust in Avalonia: examples from Newfoundland and Nova Scotia, Canada. *Canadian Journal of Earth Sciences*, **52**, 161-181, https://doi.org/10.1139/cjes-2014-0157.

Rino, S., Kon, Y., Sato, W., Maruyama, S., Santosh, M. and Zhao, D. 2008. The Grenvillian and Pan-African orogens: World's largest orogenies through geologic time, and their implications on the origin of superplume. *Gondwana Research*, **14**, 51-72, https://doi.org/https://doi.org/10.1016/j.gr.2008.01.001.

Sano, Y., Terada, K. and Fukuoka, T. 2002. High mass resolution ion microprobe analysis of rare earth elements in silicate glass, apatite and zircon: lack of matrix dependency. *Chemical Geology*, **184**, 217-230, https://doi.org/https://doi.org/10.1016/S0009-2541(01)00366-7.

Schoene, B. and Bowring, S. 2006. U-Pb systematics of the McClure Mountain syenite: Thermochronological constraints on the age of the $^{40}Ar/^{39}Ar$ standard MMhb. *Contributions to Mineralogy and Petrology*, **151**, 615-630, https://doi.org/10.1007/s00410-006-0077-4.

Schofield, D., Millar, I.L., Wilby, P. and Evans, J. 2010. A new, high precision U–Pb date from the oldest known rocks in southern Britain. *Geological Magazine*, **147**, https://doi.org/10.1017/S001675680999063X.

Schofield, D., Potter, J., Barr, S.M., Horák, J.M., Millar, I.L. and Longstaffe, F.J. 2016. Reappraising the Neoproterozoic 'East Avalonian' terranes of southern Great

Britain. *Gondwana Research*, **35**, 257-271,
https://doi.org/https://doi.org/10.1016/j.gr.2015.06.001.

Sha, L.K. and Chappell, B.W. 1999. Apatite chemical composition, determined by electron microprobe and laser-ablation inductively coupled plasma mass spectrometry, as a probe into granite petrogenesis. *Geochimica et Cosmochimica Acta*, **63**, 3861-3881, https://doi.org/https://doi.org/10.1016/S0016-7037(99)00210-0.

Shen, B., Dong, L., Xiao, S. and Kowalewski, M. 2008. The Avalon Explosion: Evolution of Ediacara Morphospace. *Science*, **319**, 81-84, https://doi.org/doi:10.1126/science.1150279.

Shields-Zhou, G.A., Porter, S. and Halverson, G.P. 2016. A new rock-based definition for the Cryogenian Period (circa 720 - 635 Ma). *Episodes*, **39**, 3-8, https://doi.org/10.18814/epiiugs/2016/v39i1/89231.

Sláma, J., Košler, J. *et al.* 2008. Plešovice zircon — A new natural reference material for U–Pb and Hf isotopic microanalysis. *Chemical Geology*, **249**, 1-35, https://doi.org/https://doi.org/10.1016/j.chemgeo.2007.11.005.

Stern, R.A., Bodorkos, S., Kamo, S.L., Hickman, A.H. and Corfu, F. 2009. Measurement of SIMS Instrumental Mass Fractionation of Pb Isotopes During Zircon Dating. *Geostandards and Geoanalytical Research*, **33**, 145-168, https://doi.org/https://doi.org/10.1111/j.1751-908X.2009.00023.x.

Strachan, R.A., Nance, R.D., Dallmeyer, R., D'Lemos, R.S., Murphy, J.B. and Watt, G.R. 1996. Late Precambrian tectonothermal evolution of the Malverns Complex. *Journal of the Geological Society*, **153**, 589-600, https://doi.org/10.1144/gsjgs.153.4.0589.

Strachan, R.A., Collins, A., Buchan, C., Nance, R.D., Murphy, J.B. and D'Lemos, R.S. 2007. Terrane analysis along a Neoproterozoic active margin of Gondwana: Insights from U-Pb zircon geochronology. *Journal of the Geological Society*, **164**, 57-60, https://doi.org/10.1144/0016-76492006-014.

Thompson, J., Meffre, S. *et al.* 2016. Matrix effects in Pb/U measurements during LA-ICP-MS analysis of the mineral apatite. *Journal of Analytical Atomic Spectrometry*, **31**, 1206-1215, https://doi.org/10.1039/c6ja00048g.

Thorpe, R.S. 1972. Possible subduction origin for two Pre-Cambrian calc-alkaline plutonic complexes from southern Britain. *Geological Society of America Bulletin*, **83**, 36-63.

Thorpe, R.S. 1979. Late Precambrian igneous activity in Southern Britain. *Geological Society, London, Special Publications*, **8**, 579-584, https://doi.org/10.1144/GSL.SP.1979.008.01.68.

Thorpe, R.S., Beckinsale, R.D., Patchett, P.J., Piper, J.D.A., Davies, G.R. and Evans, J.A. 1984. Crustal growth and late Precambrian-early Palaeozoic plate tectonic evolution of England and Wales. *Journal of the Geological Society*, **141**, 521-536, https://doi.org/10.1144/gsjgs.141.3.0521.

Tucker, R.D. and Pharaoh, T.C. 1991. U-Pb zircon ages for Late Precambrian igneous rocks in southern Britain. *Journal of the Geological Society*, **148**, 435-443, https://doi.org/10.1144/gsjgs.148.3.0435.

Valley, J.W., Cavosie, A.J. *et al.* 2014. Hadean age for a post-magma-ocean zircon confirmed by atom-probe tomography. *Nature Geoscience*, **7**, 219-223, https://doi.org/10.1038/ngeo2075.

Wiedenbeck, M., Allé, P. *et al.* 1995. Three natural zircon standards for U-Th-Pb, Lu-Hf, trace element and REE analyses. *Geostandards Newsletter*, **19**, 1-23, https://doi.org/https://doi.org/10.1111/j.1751-908X.1995.tb00147.x.

Willner, A.P., Barr, S.M., Gerdes, A., Massonne, H.J. and White, C.E. 2013. Origin and evolution of Avalonia: evidence from U-Pb and Lu-Hf isotopes in zircon from the Mira terrane, Canada, and the Stavelot-Venn Massif, Belgium. *Journal of the Geological Society*, **170**, 769-784.

Wolf, M.B. and London, D. 1994. Apatite dissolution into peraluminous haplogranitic melts: An experimental study of solubilities and mechanisms. *Geochimica et Cosmochimica Acta*, **58**, 4127-4145, https://doi.org/https://doi.org/10.1016/0016-7037(94)90269-0.

Woodcock, N., Holdsworth, R.E. and Strachan, R.A. 2012. *Geological History of Britain and Ireland*. Second ed. Wiley-Blackwell, Chichester.

Woodhead, J.D. and Hergt, J.M. 2005. A Preliminary Appraisal of Seven Natural Zircon Reference Materials for In Situ Hf Isotope Determination. *Geostandards and Geoanalytical Research*, **29**, 183-195, https://doi.org/10.1111/j.1751-908X.2005.tb00891.x.

Woodhead, J.D., Hergt, J.M., Shelley, M., Eggins, S. and Kemp, R. 2004. Zircon Hf-isotope analysis with an excimer laser, depth profiling, ablation of complex geometries, and concomitant age estimation. *Chemical Geology*, **209**, 121-135, https://doi.org/10.1016/j.chemgeo.2004.04.026.

Zhu, Z., Campbell, I.H., Allen, C.M. and Burnham, A.D. 2020. S-type granites: Their origin and distribution through time as determined from detrital zircons. *Earth and Planetary Science Letters*, **536**, 116140, https://doi.org/https://doi.org/10.1016/j.epsl.2020.116140.
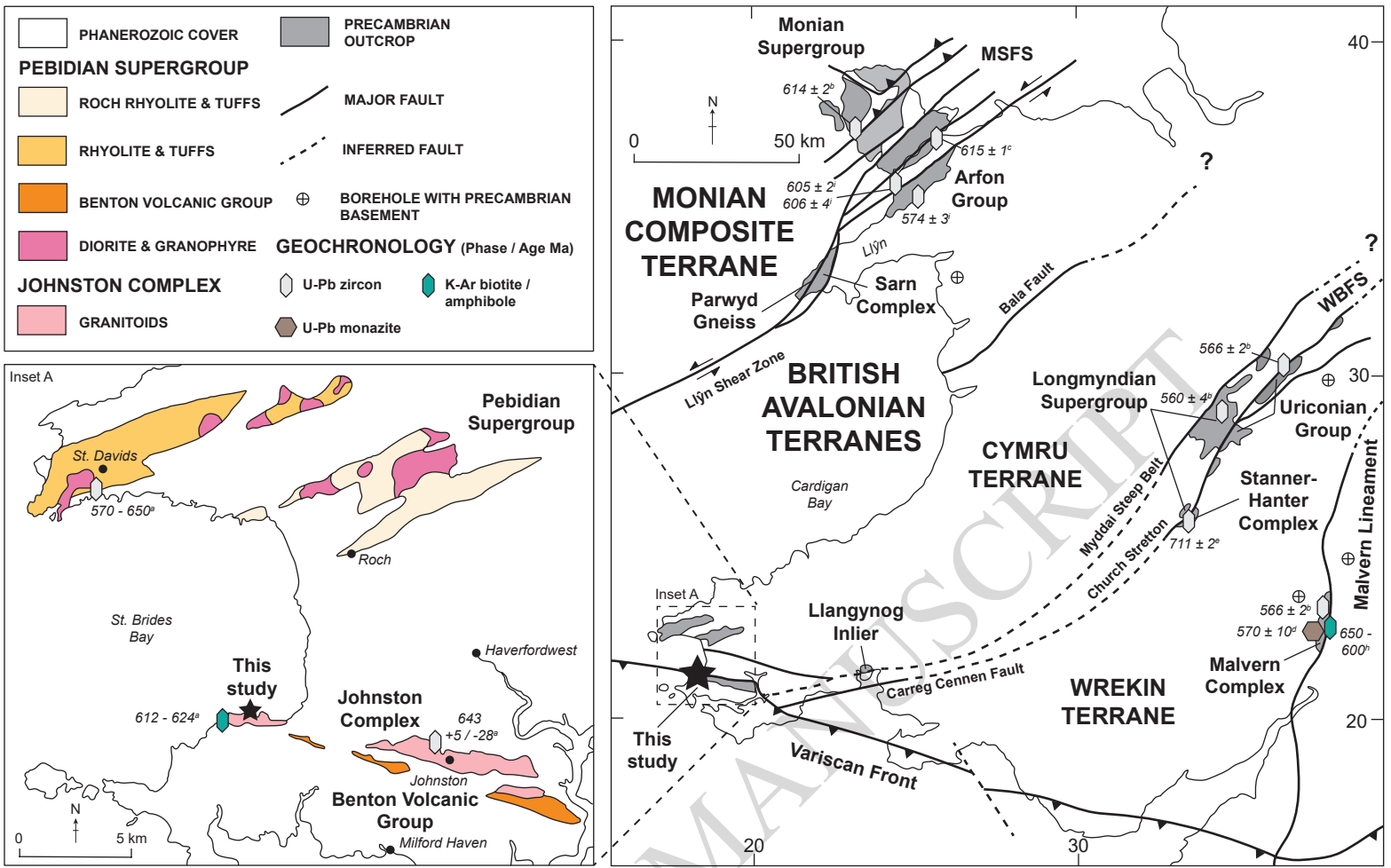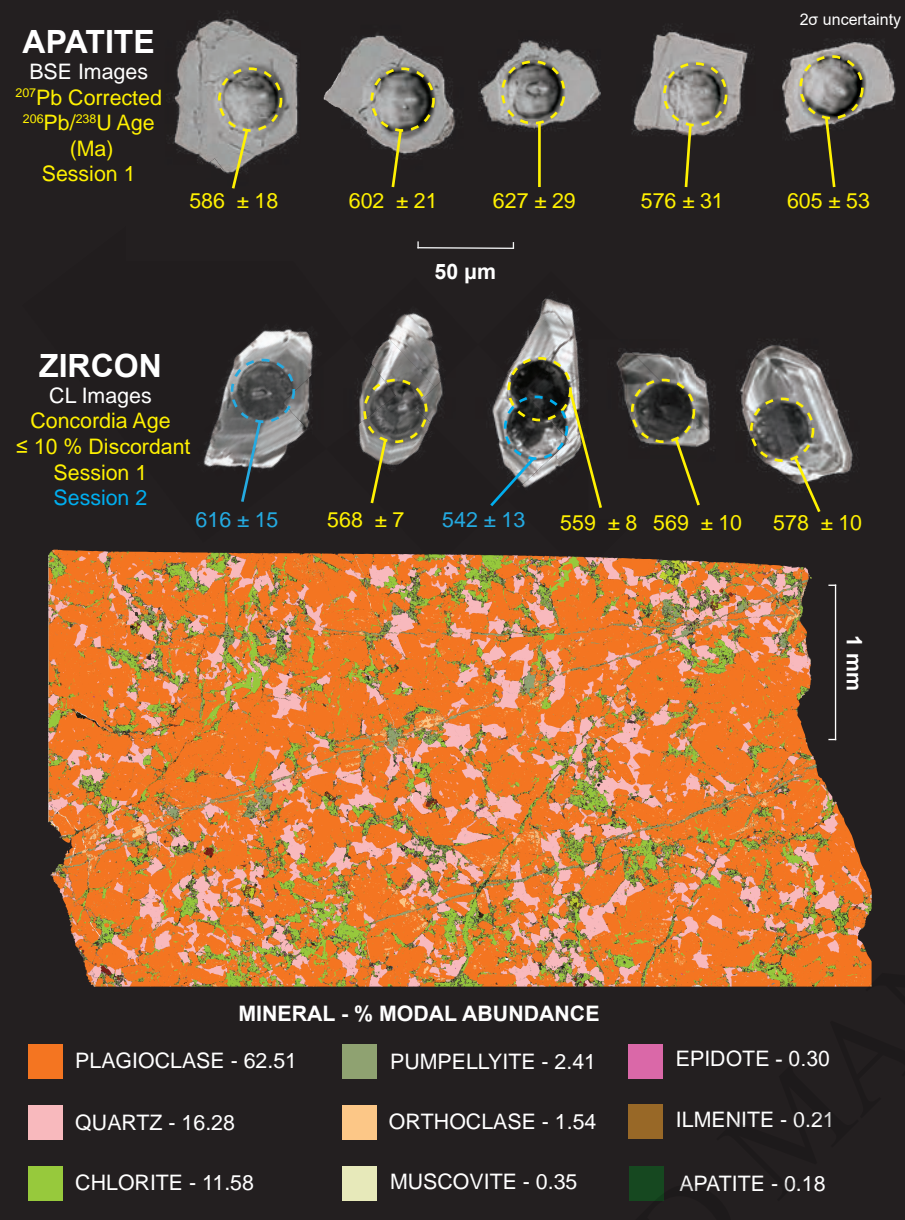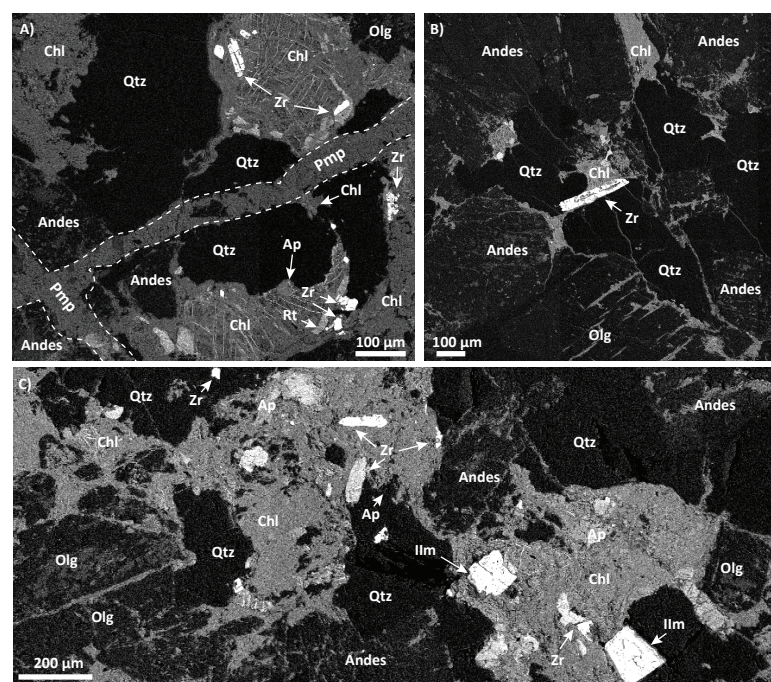
Figure 1

Figure 2

Figure 3
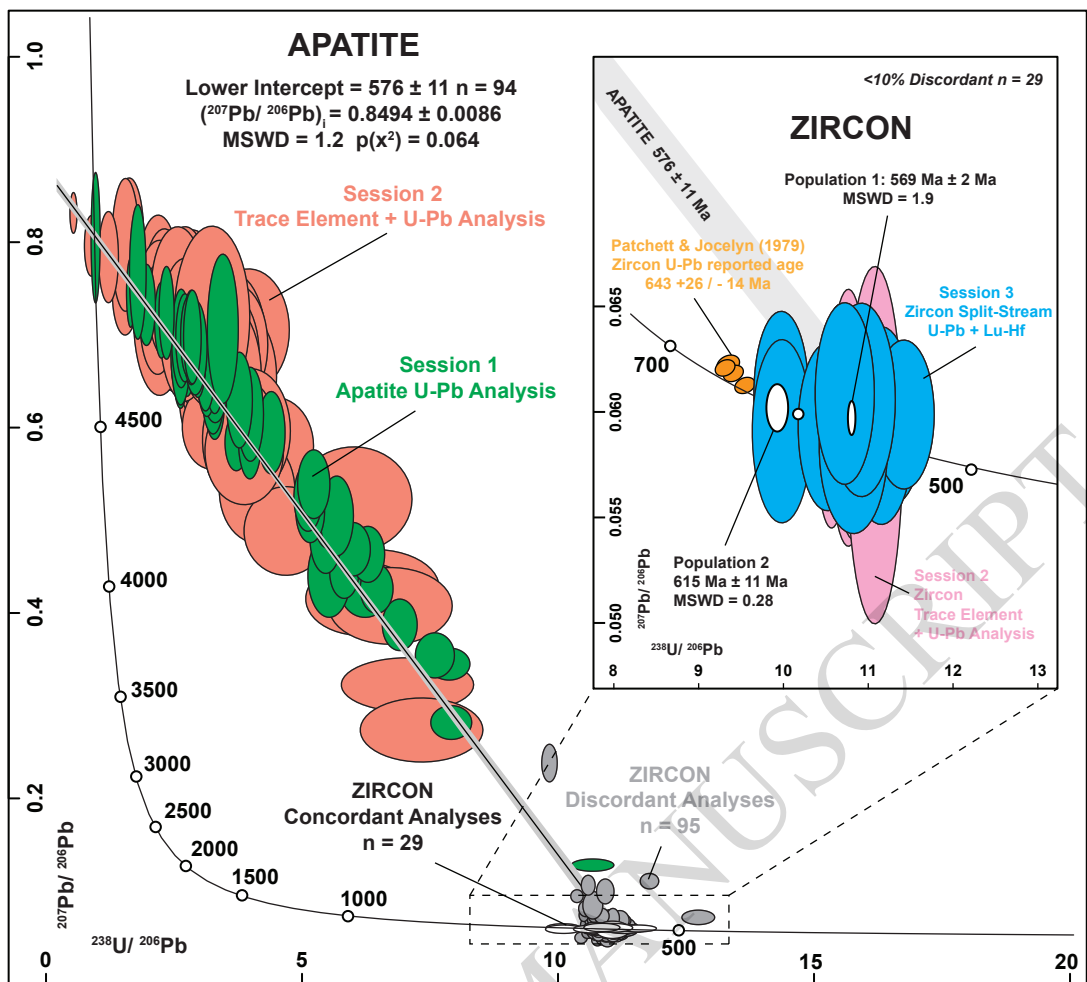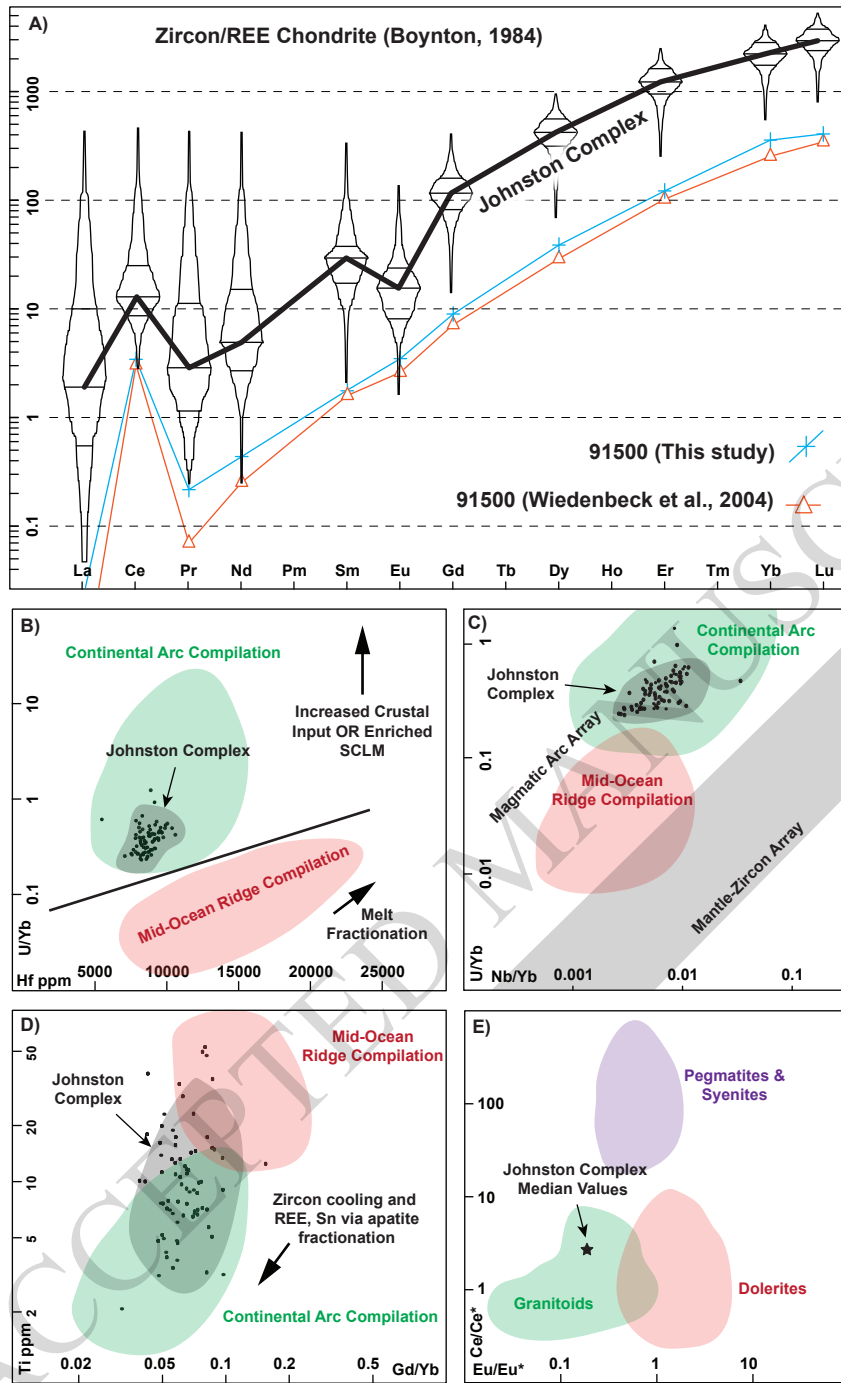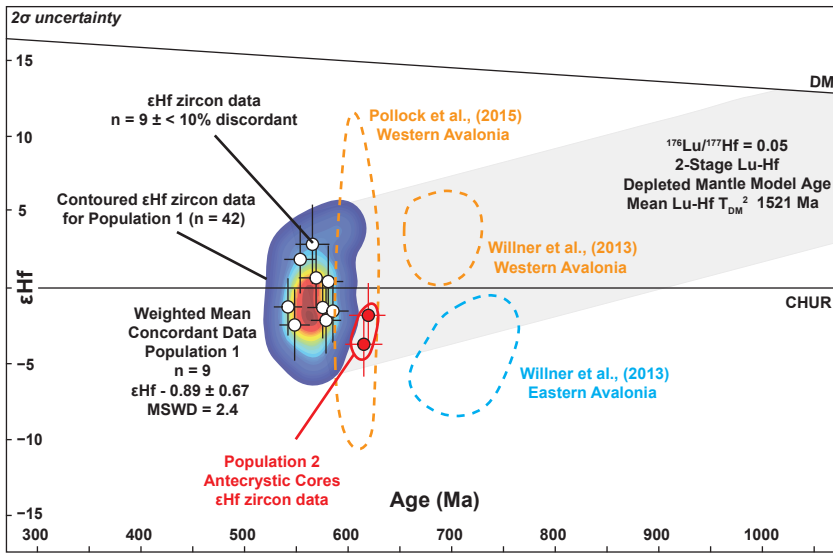
Figure 4

Figure 5

Figure 6

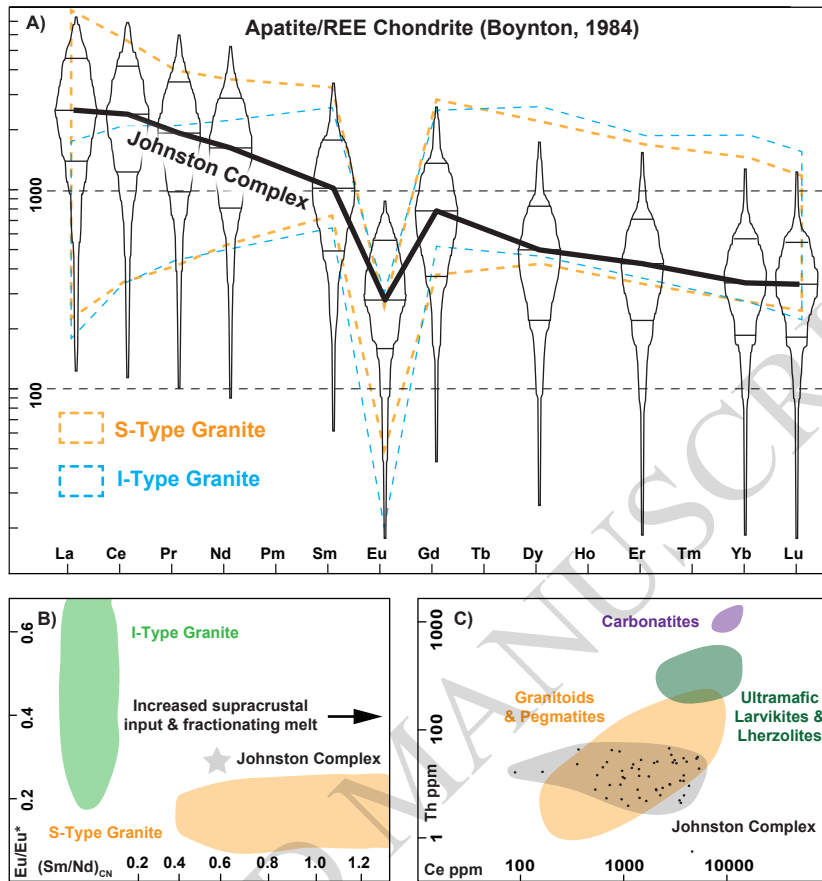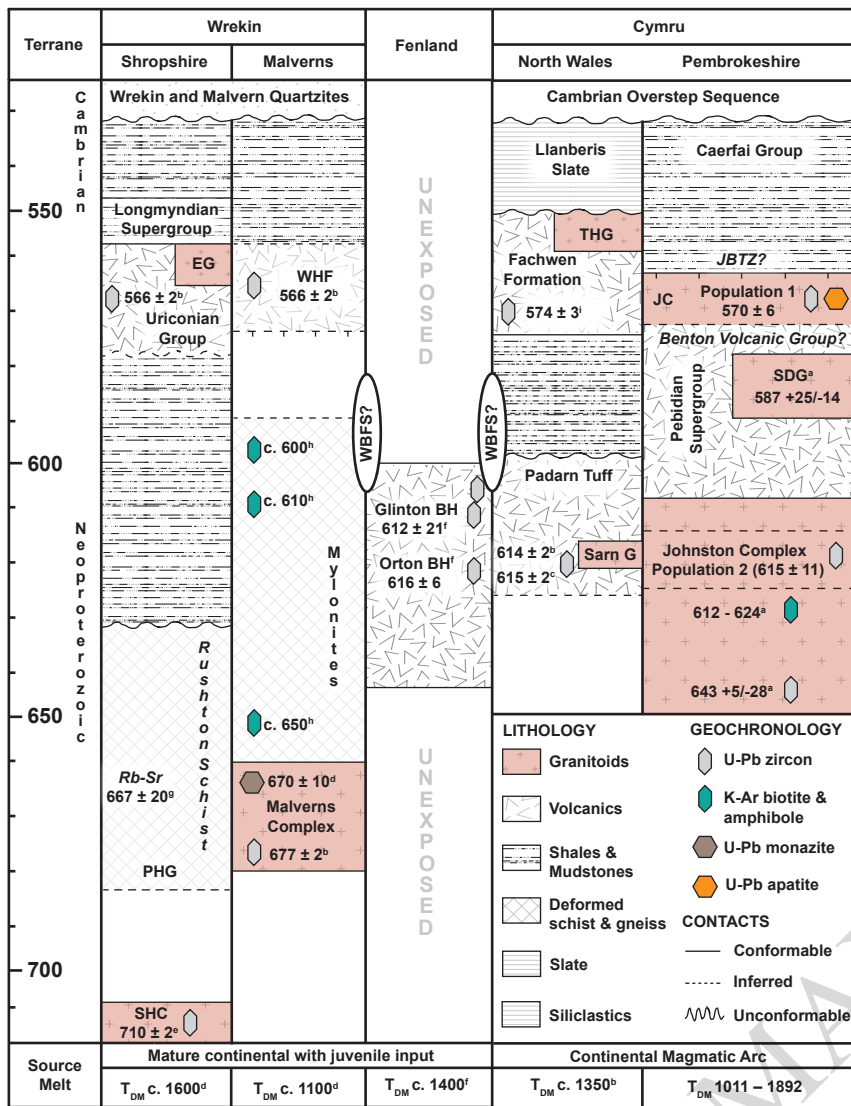Figure 7

Figure 8

1) EARLY SUBDUCTION 700 – 630 Ma

OCEANIC CRUST

JOHNSTON COMPLEX
INLAND PLUTON
643 + 5/-28 Ma
(Patchett & Jocelyn, 1979)

ACCRETIONARY WEDGE

FORE-ARC BASIN

CONTINENTAL MAGMATIC ARC

M   S-H   J

Early calc-alkaline pluton emplacement during continental arc magmatism
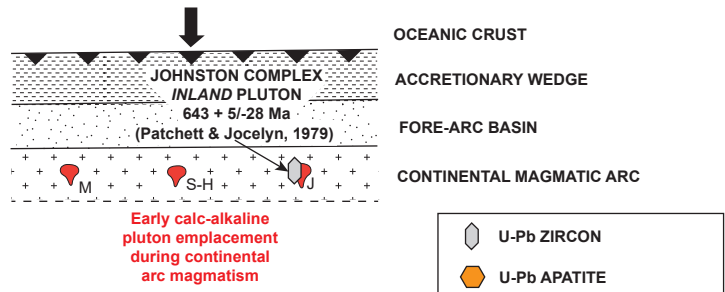
2) MAIN MAGMATIC EVENT 620 – 585 Ma

Increasingly oblique convergence & transpressive faulting

Bimodal magmatism proximal to subduction front

R

MSFL

M   S-H   J   A   S   C

ML

Ch   O-G

Extensive ca. 615 Ma magmatism across Fenland Terrane. Shared magmatic source with the Cymru Terrane?

JOHNSTON COMPLEX
COASTAL PLUTON
615 ± 11 Ma Zircon Core Age
Population 2

Legend:

⬡ U-Pb ZIRCON

⬢ U-Pb APATITE

◄— STRIKE-SLIP FAULT SHOWING RELATIVE DISPLACEMENT

⬇ RELATIVE PLATE MOVEMENT

Xx INLIER ABBREVIATION

🔴 PLUTONIC SUITES

🟢 ERUPTIVE SUITES

⬦ INACTIVE MAGMATISM

3) OBLIQUE CONVERGENCE & TERRANE DISPERSAL 570 – 550 Ma

Calc-alkaline magmatism at 570 Ma, pre terrane disperal within frontal arc slivers

Oblique convergence & terrane dispersal via strike-slip faulting

Transtensional Basin

ca. 615 Ma Zircon Core age (Population 2)

BG   R   S   B   C

MSFS   P   J   BV   A

WBFS   *ML*   U-E-L   WH   Intra-arc Basin

Dissected magmatic arc

M   S-H   Ch   O-G

JOHNSTON COMPLEX
COASTAL PLUTON
570 ± 6 Ma
Zircon (Pop. 1) & Apatite

EAST AVALONIA

Emplacement of the JC at shallow, epizonal depths within fault conduits

Figure 9